# Photodissociation Structural Dynamics of Triruthenium Dodecacarbonyl Investigated by X-Ray Transient Absorption Spectroscopy.

**ARTICLE** *in* THE JOURNAL OF PHYSICAL CHEMISTRY A · MAY 2013

Impact Factor: 2.69 · DOI: 10.1021/jp312663q · Source: PubMed



**7 AUTHORS**, INCLUDING:

Michael R Harpham
Newport Corporation
**21** PUBLICATIONS **426** CITATIONS
SEE PROFILE

Michael Mara
Northwestern University
**20** PUBLICATIONS **245** CITATIONS
SEE PROFILE

Lin X. Chen
Northwestern University
**416** PUBLICATIONS **8,434** CITATIONS
SEE PROFILE

Di-Jia Liu
Argonne National Laboratory
**93** PUBLICATIONS **1,947** CITATIONS
SEE PROFILE

THE JOURNAL OF PHYSICAL CHEMISTRY A

Article

pubs.acs.org/JPCA

# Photodissociation Structural Dynamics of TriruthenimDodecacarbonyl Investigated by X-ray Transient Absorption Spectroscopy

Michael R. Harpham,[†] Andrew, B. Stickrath,[†] Xiaoyi, Zhang,[‡] Jier Huang,[†] Michael W. Mara,[†,§] Lin X. Chen,*[,†,§] and Di-Jia Liu*[,†]

[†]Chemical Sciences & Engineering Division and [‡]Advanced Photon Source, 9700 South Cass Avenue, Argonne National Laboratory, Lemont, Illinois 60439, United States

[§]Department of Chemistry, Northwestern University, 2145 Sheridan Road, Evanston, Illinois 60208, United States

Supporting Information

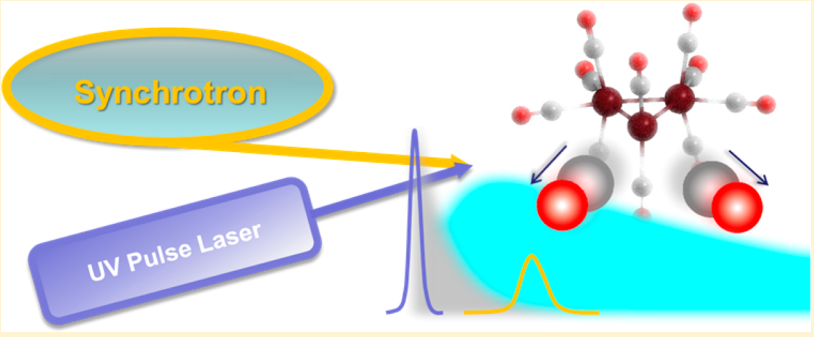


**ABSTRACT:** The molecular and electronic structures of the transient intermediates generated from the photolysis of triruthenimdodecacarbonyl, $Ru_3(CO)_{12}$, by ultrafast UV (351 nm) laser excitation were investigated using X-ray transient absorption (XTA) spectroscopy. The electronic configuration change and nuclear rearrangement after the dissociation of carbonyls were observed at ruthenium K-edge X-ray absorption near edge structure and X-ray absorption fine structure spectra. Analysis of XTA data, acquired after 100, 200, and 400 ps and 300 ns time delay following the photoexcitation, identified the presence of three intermediate species with $Ru_3(CO)_{10}$ being the most dominating one. The results set an example of applying XTA in capturing both transient electronic and nuclear configurations in metal clusters simulating catalysts in chemical reactions.

## INTRODUCTION

Triruthenimdodecacarbonyl, $Ru_3(CO)_{12}$, is among one of the most studied metal−organic complexes due to its unique molecular structure and important applications in photochemistry and homogeneous catalysis.[1−3] $Ru_3(CO)_{12}$, shown in Figure 1, has an equilateral triangle metal cluster core with each Ru atom bonded by four carbonyls.[4] The electronic transitions of $Ru_3(CO)_{12}$ in the ultraviolet and visible regions were studied by theoretical and experimental methods.[5,6] One of the most investigated aspects of $Ru_3(CO)_{12}$ is its photoactivation and photodissociation behavior. Under visible and UV radiation, $Ru_3(CO)_{12}$ undergoes various structural fragmentation and reconfiguration including Ru−Ru bond cleavage, carbonyl detachment, and formation of Ru−$\mu$(CO) bond or $Ru(CO)_5$.[7−11] In addition to the excitation by photon energy, the reconfiguration and reaction pathways depend strongly on the solvent polarizability and/or the backbonding of $\pi$-electron donating ligands such as CO, $C_2H_4$, etc.[7−11] The lifetime of the transient intermediates generated by photolysis were studied by the time-resolved infrared spectroscopy in microsecond ($\mu$s)[12] and picosecond (ps)[13] time domains. These studies focused on monitoring time-dependent behavior of CO stretching frequencies that are sensitive to the local molecular structures to gain understanding of the formation and dissipation of various photochemical intermediates through the ligand binding environments. For example, the study by Glascoe et al. identified for the first time the coexistence of two short-lived bridging carbonyl complexes, $Ru_3(CO)_{11}(\mu-CO)$ and $Ru_3(CO)_{10}(\mu-CO)$, produced from the Ru−Ru bond cleavage and the CO loss, respectively, in the noncoordinating solvent (cyclohexane) after the 266 or 400 nm laser excitation.[13] More recently, Kong et al. reported the first time-resolved synchrotron-based X-ray diffuse scattering study of $Ru_3(CO)_{12}$ in solution through a pump−probe scheme with photodissociation triggered by the laser pulse at 390 nm.[14] Using combined experimental and theoretical scattering

**Special Issue:** Oka Festschrift: Celebrating 45 Years of Astrochemistry

**Received:** December 21, 2012
**Revised:** May 21, 2013
**Published:** May 22, 2013

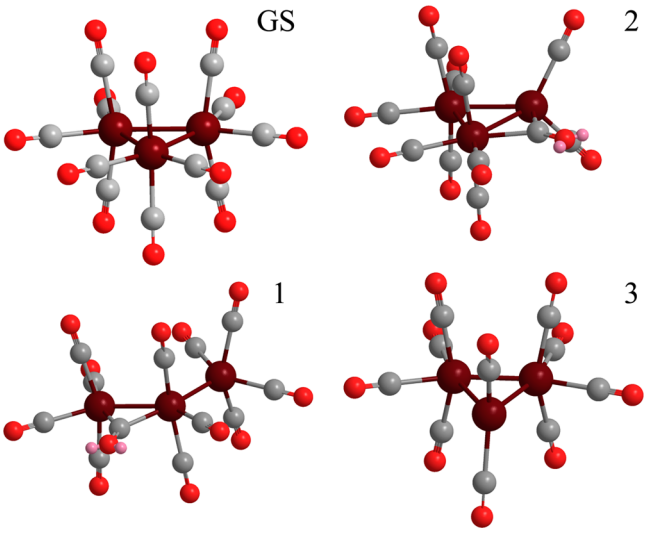


**Figure 1.** Ground state (GS) tririutheniumdodecacarbonyl and three photolysis products thought to exist on the sub-300 ns time scale based on literature reports. Ruthenium, carbon, and oxygen atoms are given in maroon, light gray, and red, respectively.

analysis, they revealed a third and more dominating component, $Ru_3(CO)_{10}$, formed by the dissociation of two CO ligands, while Ru−Ru bonds in the cluster remained intact. Since the strong scattering trimetal cluster contributed over 90% of the X-ray scattering signal, the technique is particularly sensitive to the Ru cluster structure of the photodissociation intermediates.

Different from and complementary to time-resolved IR and X-ray scattering studies, X-ray transient absorption (XTA) spectroscopy provides local structures as well as electronic configurations of the X-ray absorbing atoms.[15] In particular, one of the key information in photochemistry of transition metal complexes is the oxidation states of the metal centers along the reaction coordinates, which can be uniquely monitored by the transition edge energy and features at different probe time delays from the XTA.[15] We report here an XTA study at the ruthenium K-edge (22.117 keV) region on photodissociation chemistry of $Ru_3(CO)_{12}$ in the time scale from 100 ps to a few hundreds of nanosecond (ns) after its photoexcitation by laser pulses of 351 nm wavelength. We detected not only the structural dynamics of Ru−Ru bond-breaking, CO dissociation, and $\mu$-CO bond formation, but also identified the change of the electron distribution in 4d molecular orbitals of the Ru atoms during the course of the photodissociation reaction.

## MATERIALS AND METHODS

Tririutheniumdodecacarbonyl and cyclohexane were purchased from Aldrich and used without further purification. $Ru_3(CO)_{12}$ solutions were prepared in cyclohexane at a 1 mM concentration. The solution samples were purged with dry nitrogen gas during the entire XTA experiment.

XTA spectra were obtained at beamline 11-ID-D at the Advanced Photon Source (APS) in Argonne National Laboratory using the experimental setup previously described.[15−18] A hybrid timing mode with "top-up" operation of the synchrotron source was used where the storage ring evolution is at 271 kHz or 3.68 $\mu$s per evolution containing a "super-bunch" with 16% of the total charges and a cluster of 56 pulses with 84% of total charges well-separated by ∼1.8 $\mu$s in time from each other. The energy resolution, defined as $\Delta E/E$, was $1.4 \times 10^{-4}$. The "super-bunches" were selected as the probe pulse with the laser pulses synchronized at 1.6 kHz repetition rate. A large 400 mL volume of solution in a reservoir was continuously circulated by a peristaltic pump and flowed through a nozzle into the sample chamber to ensure that a fresh sample was illuminated with each laser shot. The entire reservoir was refreshed periodically every few hours and a fresh aliquot of solution was used for the XTA scans at each delay time. The third harmonic generation unit of a Quantronix Nd:YLF regenerative amplifier was used to produce laser pulses of wavelength 351 nm at a pulse energy of 0.22 mJ/pulse, focused to a diameter of 0.8 mm, giving a radiant exposure of ca. 0.4 mJ/mm$^2$. This spot size was chosen to be slightly larger than that of the solution jet (∼0.7 mm diameter). Laser and X-ray pulses were spatially overlapped in two steps. First, a 100 $\mu$m radius pinhole was placed in the sample chamber and aligned to the X-ray by translating the sample chamber horizontally and vertically to maximize count rate on the ion chamber located beyond the pinhole (and chamber). Second, the laser was aligned so that it was centered on the pinhole. The laser pulse was used to initiate CO photodissociation in the $Ru_3(CO)_{12}$ solution jet, while a time-delayed X-ray pulse, of ca. 100 ps duration with photon energies near the Ru K-edge (22.117 keV), was used to obtain transient X-ray absorption signal after the excitation with a known time delay. To assemble an XTA spectrum at a given time delay, Ru K-edge X-ray fluorescence was collected as a function of X-ray probe photon energy selected by a monochromator with Si(111) crystals. The signal at each chosen photon energy in the entire energy scan was averaged over 32 s integration time at each energy point, corresponding to 32 000 X-ray probe pulses, approximately $6 \times 10^5$ incident photons/pulse, or $1.8 \times 10^{10}$ total incident photons/energy point. Because of the low sample concentration, X-ray fluorescence detection was used employing a pair of detectors coupled with Z-1 filter/Soller slit/plastic scintillator/photomultiplier tubes. The ground state X-ray absorption spectra were obtained from an average of signal from the 20 X-ray pulses arriving before the laser pulse initiates the reaction (i.e., probing the material before time zero). A minimum of eight scans were collected and averaged at each time delay.

In order to further improve the signal-to-noise ratio in the XTA spectra, in situ curve fitting routine (developed by Guy Jennings) was used to process the signals of the PMTs, which was found to be crucial for low concentration samples. Because of this procedure as well as improved X-ray photon flux in an in-line dual undulator at Beamline 11-ID-D, the number of scans required for an analyzable spectrum has been reduced from 40−100 in our early studies to 8−10 in our current study.

Fitting of the Fourier-transformed XTA spectra was performed using the WinXAS 97 program[19] using standard procedures. Fourier-transformed X-ray absorption fine structure (XAFS) data were fit to the equation:

$$\chi(k) = \sum_i F_i(k) S_0^2(k) N_i/(kR_i^2) \exp(-2\sigma_i^2 k^2) \sin[2kR_i + \phi_i(k)] \quad (1)$$

where $F(k)$ is the magnitude of the backscattering, $S_0$ the amplitude reduction factor, $N$ the coordination number, $R$ the average distance, $\sigma^2$ the Debye−Waller factor, and $\phi_i$ the phase


dx.doi.org/10.1021/jp312663q | J. Phys. Chem. A 2013, 117, 9807−9813

shift; the subscript indicates the $i$th atom, and $k$ is the electron wavevector ($k = [2m(E - E_0)/h^2]^{1/2}$, $m$, electron mass; $E$, incident X-ray photon energy, $E_0$, transition edge energy; and $h$, Planck's constant). To analyze XTA results, models for the photodissociated intermediate structures were assumed based on time-resolved X-ray scattering and IR results reported by others (Figure 1).[13,14,20] The laser-excited spectra were analyzed iteratively, by first fixing the fractions of ground and (multiple) intermediate states to the ratios determined by time-resolved X-ray scattering while allowing the structure to vary from that determined by DFT, then fixing the structure while varying the fraction of each species. The procedure was repeated until the residuals were minimized. As an example of this, the preliminary fitting procedure is given for the 300 ns data:

$$\chi(k) = \alpha_1 \sum_i \chi_i(k) + \alpha_2 \sum_j \chi_j(k) \quad (2)$$

where $\alpha_1$ and $\alpha_2$ represent the fraction of ground state and excited state, respectively, and multiply the scatter $\chi(k)$ of each path associated with that species. All Ru atoms in the ground state structure are degenerate and related by a $D_{3h}$ symmetry; however, intermediate **3** has two degenerate $Ru(CO)_4$ groups and one $Ru(CO)_2$ group (Figure 1). As a result, the equation then becomes

$$\chi(k) = \alpha_1 \sum_i \chi_i(k) + \alpha_2(2 \sum_l \chi_l(k) + \sum_m \chi_m(k)) \quad (3)$$

where the subscript $l$ refers to the scattering paths associated with the $Ru(CO)_4$ groups, while the $m$ denotes scattering paths associated with the $Ru(CO)_2$ group. Hence, the resulting spectra are considered as an average not only of different possible species present at a given time delay, but also the different environments experienced by the ruthenium atoms of a given species.

## RESULTS AND DISCUSSION

X-ray absorption near-edge spectra (XANES) are given in Figure 2. The changes between ground state and laser-illuminated spectra appeared to be minor at first glance. Upon further examination, however, a trend with respect to X-ray probe time delay can be clearly and reproducibly observed in the difference spectra (defined as with laser-illumination minus without laser illumination), as is shown in Figure 2. A maximum in the difference signal between laser excited and ground state (no laser) spectra is observed at ca. 22.117 keV. This observation suggests that there is a change in electronic configuration upon the excitation. The positive change in the signal intensity at the middle of the transition edge suggests the vacancies in certain metal centered molecular orbitals created by the light excitation. The electronic configuration of $Ru_3(CO)_{12}$ ground state has been well studied.[6,21] For example, the electronic states from an extended Hückel molecular orbital calculation were constructed by Tyler et al. using three $Ru(CO)_4$ fragments of $C_{2v}$ symmetry to form $D_{3h}$ $Ru_3(CO)_{12}$.[6] In the same work, the $Ru_3(CO)_{12}$ absorption band at 390 nm was assigned to $\sigma \rightarrow \sigma^*$ transition, and the band at 320 nm to $\sigma^* \rightarrow \sigma^{*\prime}$ transition. More elaborate calculations were carried out[21] by Hunstock et al. using newer computational methods at SCF, MP2, and DFT levels of theory. In this work, the molecular orbitals were constructed[21] with three $Ru(CO)_4$ groups, each having one $\sigma$ and one $d_\pi$ hybrid frontier orbital in addition to three lower energy orbitals possessing with $t_{2g}$-like symmetry. Because the UV laser in our

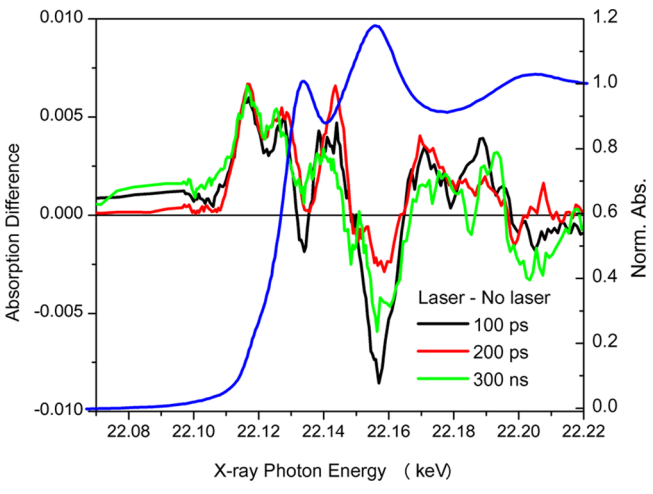


**Figure 2.** (Right axis) X-ray absorption near edge structure (XANES) region of the ground state X-ray absorption spectrum of $Ru_3(CO)_{12}$ (blue). (Left axis) Difference spectra, defined as laser-excited minus laser off (ground state) spectrum, within the XANES region at time delays 100 ps (black), 200 ps (red), and 300 ns (green).

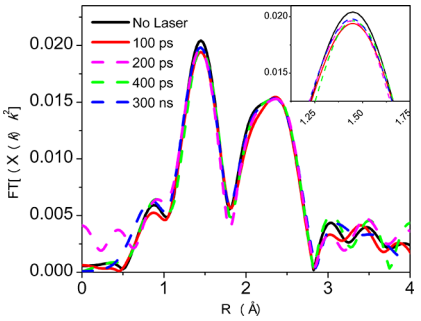


**Figure 3.** Fourier-transformed X-ray transient absorption (XTA) spectra with $k2$ weighting are plotted against distance R in Å, including ground state (no laser, black), and the results from time delays between laser pump and X-ray probe of 100 ps (red), 200 ps (magenta), 400 ps (green), and 300 ns (blue), respectively. Inset: As above, zoomed in to show the left edge of the 1st peak.

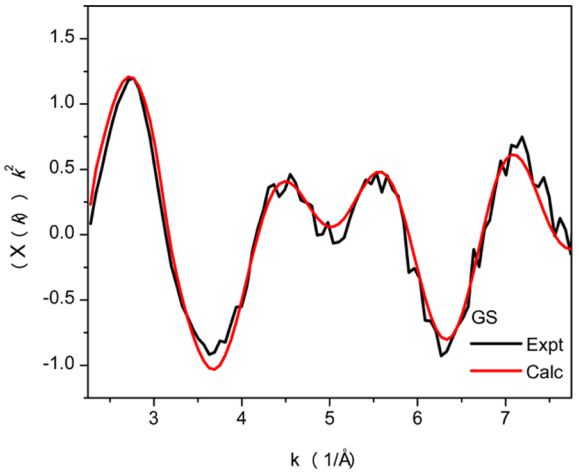


**Figure 4.** Comparison between the experimental (black) and calculated (red) $k$-space spectra of ground state $Ru_3(CO)_{12}$.


dx.doi.org/10.1021/jp312663q | J. Phys. Chem. A 2013, 117, 9807−9813

**Table 1. Structural Parameters of Photolysis Products and Ground State of $Ru_3(CO)_{12}$ As Determined from Fitting of X-ray Transient Absorption Data**

| | | scattering paths | | | | | | | | | | | | |
|---|---|---|---|---|---|---|---|---|---|---|---|---|---|---|
| | | Ru−C | | | R−C mu | | | Ru−Ru | | Ru−Ru #2 | | Ru−O | | |
| species | Ru environment[a] | $N$[b] | $R$[c] (Å) | $\sigma^{2d}$ ($10^{-3}$ Å$^2$) | $N$ | $R$ (Å) | $\sigma^2$ ($10^{-3}$ Å$^2$) | $R$ (Å) | $\sigma^2$ ($10^{-3}$ Å$^2$) | $R$ (Å) | $\sigma^2$ ($10^{-3}$ Å$^2$) | $N$ | $R$ (Å) | $\sigma^2$ ($10^{-3}$ Å$^2$) |
| Int 1 | $(CO)_4$ mu−CO | 4 | 1.95 | 5.3 ± 0.5 | 1 | 2.11 | 6.2 ± 0.2 | 2.83 | 3.9 ± 0.6 | | | 4 | 3.14 | 6.0 ± 0.4 |
| | $(CO)_3$ mu−CO | 3 | 1.92 | 4.5 ± 0.2 | 1 | 2.02 | 0.9 ± 0.3 | 2.82 | 3.8 ± 0.4 | 3.05 | 3.0 ± 0.2 | 3 | 3.14 | 7.0 ± 0.4 |
| | $(CO)_4$ | 4 | 1.95 | 4.4 ± 0.3 | | | | 2.97 | 2.1 ± 0.2 | | | 4 | 3.15 | 9.0 ± 0.3 |
| Int 2 | $(CO)_4$ | 4 | 1.94 | 1.9 ± 0.2 | | | | 2.78 | 0.9 ± 0.2 | 2.79 | 3.3 ± 0.1 | 4 | 3.13 | 5.0 ± 0.4 |
| | $(CO)_2$ mu−CO | 2 | 1.93 | 0.6 ± 0.2 | 1 | 2.01 | 1.5 ± 0.2 | 2.74 | 1.9 ± 0.1 | 2.78 | 2.3 ± 0.1 | 3 | 3.27 | 9.5 ± 0.3 |
| | $(CO)_4$ mu−CO | 4 | 1.94 | 2.3 ± 0.3 | 1 | 2.12 | 6.2 ± 0.4 | 2.82 | 4.2 ± 0.3 | 2.77 | 1.5 ± 0.3 | 4 | 3.14 | 3.1 ± 0.3 |
| Int 3 | $(CO)_4$ | 4 | 1.94 | 1.3 ± 0.4 | | | | 2.67 | 6.0 ± 0.4 | 2.89 | 7.7 ± 0.9 | 4 | 3.06 | 6.2 ± 0.4 |
| | $(CO)_2$ | 2 | 1.94 | 0.7 ± 0.2 | | | | 2.67 | 5.8 ± 0.9 | | | 2 | 3.24 | 8.7 ± 0.6 |
| GS | $(CO)_4$ | 4 | 1.93 | 2.7 ± 0.3 | | | | 2.85 | 7.3 ± 0.9 | | | 4 | 3.15 | 7.9 ± 0.3 |

[a]CO groups nearest-neighbor to the absorbing ruthenium atom. [b]Coordination number. [c]Distance of scatterer from Ru absorber, with experimental errors estimated at 0.02 Å. The fitting routine calculated error in distanceis in the range of ±0.002−0.02 Å; however, this is performed with multiple parameters frozen, and visible changes to the spectrum were typically observed only when a given distance was varied by ±0.01−0.02 Å, so we have chosen 0.02 Å as a more reasonable estimate of the precision of this parameter. [d]Mean-squared displacement. Errors in $\sigma^2$ for a given species are estimated by freezing all $R$ and $N$, as well as $\sigma^2$ from other species.

experiment has a wavelength of 351 nm, in the middle of $\sigma \rightarrow \sigma^*$ and $\sigma^* \rightarrow \sigma^{*\prime}$ bands, electronic transitions from both $\sigma$ and $\sigma^*$ states are involved in the photoexcitation, leading to the rearrangement of carbonyl groups to bridging positions as well as the detachment of one or two COs from the complex.[14,20] In all cases, the electronic energy levels of the new complexes are expected to undergo rearrangement due to the changes in symmetry and directionality of metal−ligand interactions, leading to the formation of unoccupied orbitals at lower energy levels, hence the observation of new features in the middle of the transition edge. From the recent scattering studies[14,20] and our result discussed below, it is suggested that the most dominant intermediate species induced by the laser excitation is the CO dissociated complex $Ru_3(CO)_{10}$, a simplification to the discussion by attributing the electronic state to only this intermediate could be made. At present, the energy level distribution of $Ru_3(CO)_{10}$ has not been reported. However, its Group VIIIA analogue $Fe_3(CO)_{10}$ has been calculated.[22] New unoccupied orbitals below that of $Fe_3(CO)_{12}$ were found as the result of eliminating two terminal carbonyls. One would expect a similar change of valence orbitals should also occur during the formation of terminal $Ru_3(CO)_{10}$ after the photodissociations of two carbonyls from $Ru_3(CO)_{12}$. Therefore, the X-ray pulse following laser excitation will promote core electron transitions into the newly vacated, lower energy orbitals, leading to a red shift of the transition near the Ru K-edge. This appears to be what we observed in the difference XANES spectra shown in Figure 2. The appearance of two peaks at 22.116 and 22.123 keV can be observed in the difference spectrum, further confirming the presence of new unoccupied orbitals in the transient species of $Ru_3(CO)_{10}$. Besides the new features arising in the middle of the Ru K-edge, two features above the transition edge, near 22.130 and 22.157 keV, reduced their intensities upon photoexcitation of the sample. These two features are typically associated with Ru(0) K-edge XANES spectra.[23] The reduction of their contributions to XANES spectra is consistent with an apparent shift of the oxidation state of Ru from 0 to +4.

The Fourier-transformed XAFS spectra are given in Figure 3. Although the difference is subtle from one delay time to another, the reduction of the first peak intensity is clearly observed. This peak corresponds to Ru−C scattering paths. A decrease in intensity upon laser excitation is consistent with the dissociation of CO. A slight shift to longer distances is also observed in the 100−400 ps delays, which is consistent with the elongation of the Ru−C bond in a $\mu$-CO group. The second peak corresponds to Ru−Ru and Ru−O scattering paths as well as multiple scattering paths. At 100 ps, the intensity at lower R value of the second peak is found to decrease, suggesting a shift to a longer bond distance. This observation is consistent with the model of Ru−Ru bond breaking/CO dissociation as well as bond lengthening. Some recovery of the ground state species can be observed in the 300 ns data.

The following steps were taken in the fitting of XAFS spectra. The ground state spectra were fit first, as the $D_{3h}$ symmetry of the molecule meant that only one kind of Ru site with four CO ligands and two Ru−Ru bonds needed to be considered. The $k$-space results are shown in Figure 4, and the fitted parameters are given in Table 1. Ru−Ru distances were found to be 2.85 Å, similar to the crystal structure,[4] and shorter by 0.03 and 0.08 Å than those observed in scattering measurements[14,20] and DFT,[13] respectively. Ru−C were found to be 1.95 Å, in close agreement with the crystal structure[4] and DFT results[13] obtained by others. On the basis of their agreement with reported values, these structural parameters were used as the references in our fitting of the photogenerated intermediates.

According to the previous studies,[14,20] at least three intermediate structures are known to exist after the photoexcitation. At 300 ns delay, however, only intermediate **3**, in addition to ground state material, has been shown to exist in significant quantity. Thus, being the simplest case, the 300 ns delay is chosen as the starting point for the analysis of our time-resolved data. To obtain structural data, the 300 ns data is first fitted by the WinXAS 97 program[19] as detailed in the previous section to a weighted sum of the scattering paths for the two types of ruthenium environments (one is the same as in the ground state, with two Ru−Ru bonds and four Ru−CO, and the other has two Ru−Ru bonds with only two Ru−CO), allowing variation of the fraction of excited state and ground state and refinement of the structure of intermediate **3**. This refinement, coupled to that of the ground state can then be used as a starting point for the earlier time delays, in which


dx.doi.org/10.1021/jp312663q | J. Phys. Chem. A 2013, 117, 9807−9813

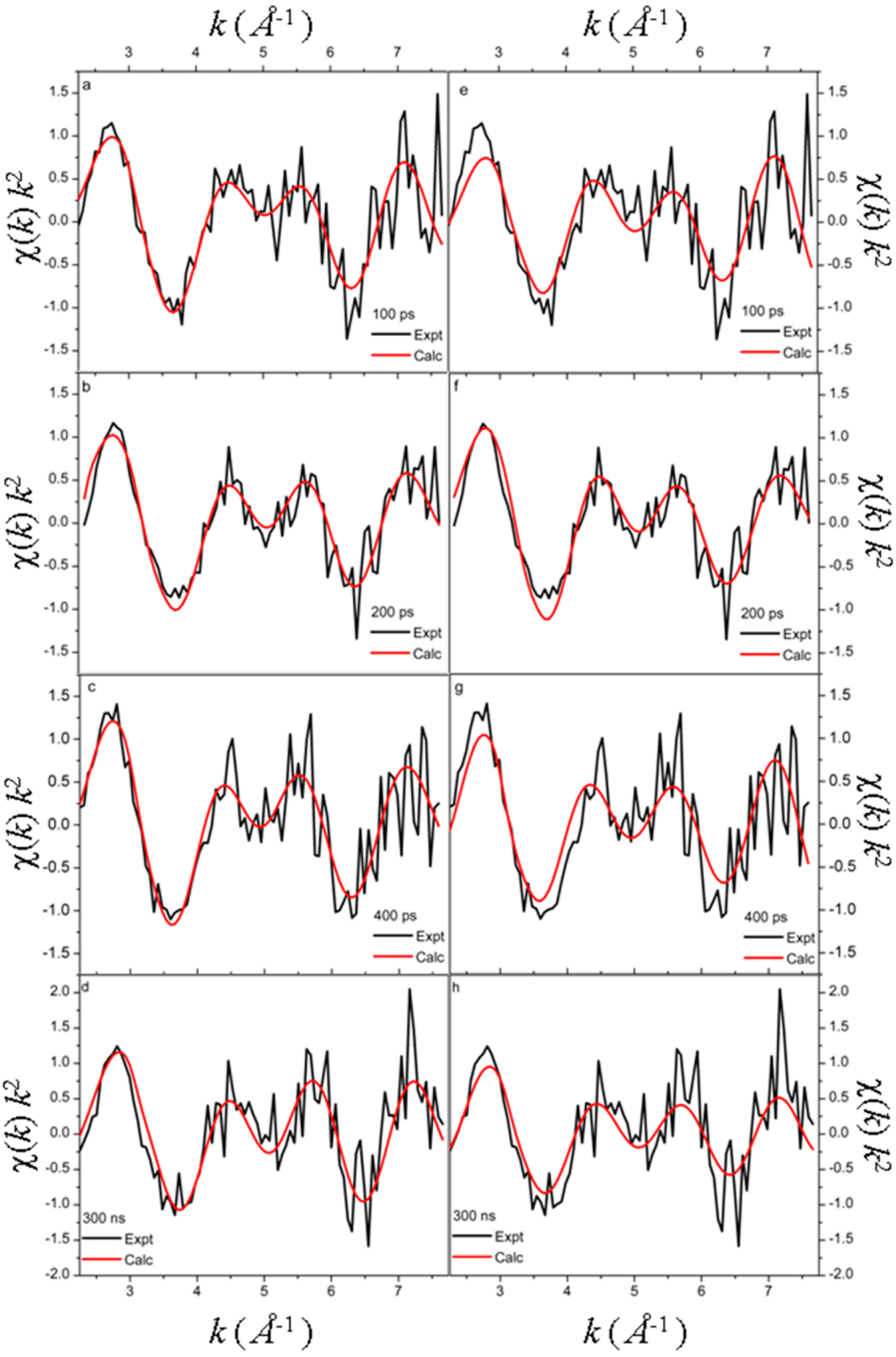


**Figure 5.** *k*-Space spectra obtained after photoexcitation of $Ru_3(CO)_{12}$ by 351 nm light at various time delays. Experimental results are given in black, while spectra calculated by fitting to ground state plus all intermediates (panels a–d) or by fitting to ground state plus intermediate **3** (panels e–h) are given in red.

additional intermediates are thought[14,20] to be present. As a first attempt of fitting the data at 100 ps time delay, a delay limited by the time resolution of the experiments, the transient spectra is fitted using only two structures, corresponding to the ground state and intermediate **3**, with the structural parameters obtained from fitting the spectra at 300 ns delay time, and the fractions of ground state and intermediate **3**. However, satisfactory results were not obtained from this simplistic approach. Therefore, the other two intermediates, which were previously reported[14,20] to be present, were then added. The resulting spectrum is fitted by a summation of three spectra each for intermediates **1** and **2** and two for intermediate **3**


dx.doi.org/10.1021/jp312663q | J. Phys. Chem. A 2013, 117, 9807–9813

**Table 2. Percentages of Species Existing at Various Delays between Laser Pump and X-ray Probe As Determined by Analysis of Fourier-Transformed X-ray Absorption Spectra**

| species[a] | 100 ps | 200 ps | 400 ps | 300 ns |
|---|---|---|---|---|
| Int1 | 6.0 ± 0.1% | 2.0 ± 0.2% | 2.0 ± 0.2% | 2.0 ± 0.2% |
| Int2 | 9.0 ± 0.2% | 8.0 ± 0.1% | 8.0 ± 0.1% | 2.0 ± 0.2% |
| Int3 | 19.0 ± 0.5% | 19.0 ± 0.3% | 19.0 ± 0.3% | 12.0 ± 0.1% |
| GS | 66.0 ± 0.3% | 70.0 ± 0.2% | 70.0 ± 0.2% | 84.0 ± 0.2% |

[a]Species GS refers to unexcited, ground state material, while Int1, Int2, and Int3 refer to photolysis intermediates displayed in Figure 1. The percentage of a given species multiplies the coordination number for each scattering path associated with that species. Errors are *estimated* with all distances and mean-squared displacements frozen and should be taken as estimates around a minimum.

(from the symmetry, identical spectra are produced by two of the ruthenium atoms of the intermediate), for a total of eight sets of scattering paths and their associated parameters. As varying the parameters from all scattering paths simultaneously would represent a significant overdetermination of the data, fitting is accomplished in stages. Following the aforementioned fit of the 300 ns data to intermediate **3** plus ground state, scattering paths for the ruthenium atoms in intermediates **1** and **2** were added, and optimization was performed with the geometries for intermediate **3** and ground state frozen at our previously determined values. The quality of the fit for the 300 ns data was observed to slightly improve when these other intermediates were added; however, their relative contribution was small, 2−3% each of the total signal, in agreement with other reports.[14] Using the intermediate **3** and ground state geometries optimized at 300 ns, the 100, 200, and 400 ps time-delay data were each fit to a sum of the scattering paths for all three of the intermediates present plus the ground state. The *k*-space plots of the data and fits are given in Figure 4 for the ground state $Ru_3(CO)_{12}$ and Figure 5 for X-ray probe at various time delays after laser excitation. Fits with all species contributing are shown in the left panels (a−d) of Figure 5, while intermediates **1** and **2**, both of which were individually found have <10% fractional contribution to the total spectrum, are omitted from fitting (with parameters in intermediate **3** and ground state refit) in the right panel figures (e−h). It can be observed that, with the possible exception of 300 ns delay (Figure 5d,h), the fit is improved by the addition of intermediates **1** and **2** and optimization of parameters. The optimized structural parameters associated with Figure 5e−h (all species contributing) are given in Table 1. Trends in Ru−Ru distances are found to agree well with those reported by others.[13,14,20] It is observed that Ru−Ru distance decreases (relative to ground state $Ru_3(CO)_{12}$) for Ru atoms sharing a $\mu$−CO group, as in intermediates **1** and **2**, with the remaining Ru−Ru bond length extending. For these intermediates, the $\mu$−CO group is found to be located closer to the Ru atom "donating" that group, and also possessing fewer "unshared" CO groups, which is a result that could not be determined from the time-resolved X-ray scattering results published by others.[14,20] For the double-CO-loss intermediate **3**, the $Ru(CO)_2$−$Ru(CO)_4$ distance is decreased significantly by ∼0.2 Å, while the $Ru(CO)_4$−$Ru(CO)_4$ distance is largely unchanged (0.02 Å shorter than GS); this was observed by others.[13,14,20] Given the large number of parameters, errors for the mean-squared displacements ($\sigma^2$) for a given intermediate were estimated by freezing all distances and coordination numbers as well as $\sigma^2$ for any other species, and the actual error is likely to be larger than that given in the table based on the correlation between the $\sigma^2$ parameters. Errors in distance for intermediate species are similarly difficult to quantify, however, a change of 0.02 Å in any scattering path for any species is immediately visible in the *k*-space or Fourier-transformed (*R*-space) spectrum. Thus, structural parameters associated with the intermediate species should be considered as precise, but not necessarily accurate, to 0.02 Å.

Excited and ground state fractions determined by the fitting procedures are given in Table 2 and are similar to those observed by others.[14] The excited state fractions of all species obtained from the 200 and 400 ps delay spectra are nearly identical to each other. Intermediate **1** is found to have a moderate contribution (6%) to the signal in the spectrum corresponding to 100 ps time delay, but uniformly small, possibly negligible, 2% contribution at later time delays. Intermediates **2** and **3** are found to be nearly invariant at 8% and 19%, respectively, in the 100−400 ps delay scans; however, both decrease significantly in the later 300 ns time delay. As fitting is performed in stages, with some parameters frozen, while others are optimized, errors reported in the table are estimated based on the frozen, optimized geometries, with the fractional contribution of a species multiplying the coordination number of all scattering paths relevant to that species. As such, even a relative change of 2% to one species (e.g., 6.1% vs 6.0%) can be observed to have a detrimental impact on the *k*-space or Fourier-transformed data. Thus, these percent contributions should, like the structural parameters, be taken as precise but not necessarily accurate.

## ■ CONCLUSIONS

X-ray transient absorption (XTA) spectroscopy was used to probe the structure and electronic configuration of intermediates generated by 351 nm, 0.22 mJ/pulse, laser-excitation of $Ru_3(CO)_{12}$ at 100, 200, and 400 ps and 300 ns time delay. The ability of XTA to study photoinduced changes in the electronic state as well as in the structure of materials on the hundreds of picoseconds to hundreds of nanoseconds time scale was showcased in this work. The XTA technique was found to be sensitive to changes in Ru−C and Ru−O distances, which were not observed by others in their time-resolved X-ray scattering methods. The electronic rearrangement after loss of CO (and electrons in Ru $e_g$ orbitals) was observed in the Ru K-edge region. Fourier-transformed XTA data were fit to a sum of the contribution of unexcited material and a set of intermediate species. Of the three intermediate species identified by others[13,14,20] as existing on the studied time scale, intermediate **3**, the double-CO-loss species, was observed to be present in the largest fraction at all studied time delays, while intermediate **1** was only found to contribute significantly at 100 ps time delay. Intermediate **3** was found to be the only species of consequence on the hundreds of nanoseconds time scale.

The intracluster Ru−Ru distances were found to be similar to those observed by the DFT and X-ray scattering measurements of others; however, our XTA experiments were capable of resolving Ru−C and Ru−O distance changes in addition. As a result of our detailed structural analysis of the intermediate species over our time range, it was found that upon CO loss, the distance between the CO-deficient Ru and the neighboring Ru decreases. Shared or $\mu$-CO groups were found to be slightly closer to the CO-deficient Ru, although at longer distance from Ru atoms than the unshared CO groups.

## ■ ASSOCIATED CONTENT

### Supporting Information

An automated F-test for XTA data analysis in R-space. This material is available free of charge via the Internet at http://pubs.acs.org.

## ■ AUTHOR INFORMATION


### Corresponding Author

*(L.X.C.) E-mail: lchen@anl.gov. Tel: (+)1-630-252-3533. (D.-J.L.). E-mail: djliu@anl.gov. Tel: (+)1-630-252-4511.


### Notes

The authors declare no competing financial interest.

## ■ ACKNOWLEDGMENTS

This contribution is dedicated to Professor Takeshi Oka, a celebrated scientist, educator, and, among many other important recognitions, the discoverer of $H_3^+$, the smallest equilateral triangle molecule. This work was supported by the Office of Science of the Department of Energy under Contract No. DE-AC02-05CH11231. The use of the Advanced Photon Source was supported by the U.S. Department of Energy, Office of Science, Office of Basic Energy Sciences, under Contract No. DE-AC02-06CH11357. The chemistry laboratory facilities used in this research are supported by funding from the U.S. Department of Energy, Office of Science, Basic Energy Sciences under Contracts DE-AC02-06CH11357.

## ■ ABBREVIATIONS

XTA, X-ray transient absorption; PMT, photomultiplier tube; XANES, X-ray absorption near-edge structure; GS, ground state; DFT, density functional theory

## ■ REFERENCES


(1) Dyson, P. J.; McIndoe, S. J. *Transition Metal Carbonyl Cluster Chemistry*; Gordon and Breach: Amsterdam, The Netherlands, 2000.

(2) Graff, J. L.; Sanner, R. D.; Wrighton, M. S. Photoactivation Of Cluster Catalysis: Comparison Of 1-Pentene Isomerization by Tetracarbonyl(triphenylphosphine)ruthenium and 1,1,1,2,2,2,3,3,3-Nonacarbonyl-1,2,3-tris(triphenylphosphine)-triangulo-triruthenium. *J. Am. Chem. Soc.* **1979**, *101*, 273−275.

(3) Richmond, M. G. Annual Survey of Organometallic Metal Cluster Chemistry for the Year 2002. *Coord. Chem. Rev.* **2004**, *248*, 881−901.

(4) Churchill, M. R.; Hollander, F. J.; Hutchinson, J. P. Accurate Redetermination of Structure of Triruthenium Dodecacarbonyl, $Ru_3(Co)_{12}$. *Inorg. Chem.* **1977**, *16*, 2655−2659.

(5) Delley, B.; Manning, M. C.; Ellis, D. E.; Berkowitz, J.; Trogler, W. C. Spectroscopic and Theoretical-Studies of Metal Cluster Complexes 0.2. X-Alpha Calculations and Spectroscopic Studies of Triruthenium and Triosmium Dodecacarbonyls. *Inorg. Chem.* **1982**, *21*, 2247−2253.

(6) Tyler, D. R.; Levenson, R. A.; Gray, H. B. Electronic-Structures and Spectra of Trinuclear Carbonyl-Complexes. *J. Am. Chem. Soc.* **1978**, *100*, 7888−7893.

(7) Bentsen, J. G.; Wrighton, M. S. Wavelength-Dependent, Medium-Dependent, and Temperature-Dependent Competition between Photosubstitution and Photofragmentation in $Ru_3(Co)_{12}$ and $Fe_3(Co)_{12}$: Detection and Characterization of Coordinatively Unsaturated $M_3(Co)_{11}$ Complexes. *J. Am. Chem. Soc.* **1987**, *109*, 4530−4544.

(8) Desrosiers, M. F.; Ford, P. C. Photochemical Fragmentation of the Cluster $Ru_3(Co)_{12}$: Evidence Against Homolytic Bond-Cleavage. *Organometallics* **1982**, *1*, 1715−1716.

(9) Desrosiers, M. F.; Wink, D. A.; Ford, P. C. Flash-Photolysis of Triruthenium Dodecacarbonyl: Evidence for Intermediates in the Competing Fragmentation and Ligand-Substitution Photoreactions of $Ru_3(CO)_{12}$. *Inorg. Chem.* **1985**, *24*, 1−2.

(10) Malito, J.; Markiewicz, S.; Poe, A. Photochemical Fragmentation Kinetics of Triruthenium Dodecacarbonyl. *Inorg. Chem.* **1982**, *21*, 4335−4337.

(11) Wuu, Y. M.; Bentsen, J. G.; Brinkley, C. G.; Wrighton, M. S. Photochemical Formation of Mononuclear Bis(ethylene) and Tris-(ethylene) Complexes from Irradiation of Iron Pentacarbonyl or Triruthenium Dodecarbonyl: Species Involved in Catalytic Alkene Isomerization. *Inorg. Chem.* **1987**, *26*, 530−540.

(12) Grevels, F. W.; Klotzbucher, W. E.; Schrickel, J.; Schaffner, K. Short-Wavelength Flash Photolytic Fragmentation of $Ru_3(Co)_{12}$ in the Presence of Co and Complementary Experiments with $Ru(Co)_5$: A Time-Resolved IR Spectroscopic Study. *J. Am. Chem. Soc.* **1994**, *116*, 6229−6237.

(13) Glascoe, E. A.; Kling, M. F.; Shanoski, J. E.; Harris, C. B. Nature and Role of Bridged Carbonyl Intermediates in the Ultrafast Photoinduced Rearrangement of $Ru_3(CO)_{12}$. *Organometallics* **2006**, *25*, 775−784.

(14) Kong, Q.; Lee, J. H.; Plech, A.; Wulff, M.; Ihee, H.; Koch, M. H. J. Ultrafast X-ray Solution Scattering Reveals an Unknown Reaction Intermediate in the Photolysis of $Ru_3(CO)_{12}$. *Angew. Chem., Int. Ed.* **2008**, *47*, 5550−5553.

(15) Chen, L. X.; Jager, W. J. H.; Jennings, G.; Gosztola, D. J.; Munkholm, A.; Hessler, J. P. Capturing a Photoexcited Molecular Structure through Time-Domain X-ray Absorption Fine Structure. *Science* **2001**, *292*, 262−264.

(16) Chen, L. X.; Jennings, G.; Liu, T.; Gosztola, D. J.; Hessler, J. P.; Scaltrito, D. V.; Meyer, G. J. Rapid Excited-State Structural Reorganization Captured by Pulsed X-rays. *J. Am. Chem. Soc.* **2002**, *124*, 10861−10867.

(17) Chen, L. X.; Shaw, G. B.; Novozhilova, I.; Liu, T.; Jennings, G.; Attenkofer, K.; Meyer, G. J.; Coppens, P. MLCT State Structure and Dynamics of a Copper(I) Diimine Complex Characterized by Pump−Probe X-ray and Laser Spectroscopies and DFT Calculations. *J. Am. Chem. Soc.* **2003**, *125*, 7022−7034.

(18) Harpham, M. R.; Nguyen, S. C.; Hou, Z.; Grossman, J. C.; Harris, C. B.; Mara, M. W.; Stickrath, A. B.; Kanai, Y.; Kolpak, A. M.; Lee, D.; Liu, D.-J.; Lomont, J. P.; Moth-Poulsen, K.; Vinokurov, N.; Chen, L. X.; Vollhardt, K. P. C. X-ray Transient Absorption and Picosecond IR Spectroscopy of Fulvalene(tetracarbonyl)diruthenium on Photoexcitation. *Angew. Chem., Int. Ed.* **2012**, *51*, 7692−7696.

(19) Ressler, T. WinXAS: A New Software Package Not Only for the Analysis of Energy-Dispersive XAS Data. *J. Phys. IV* **1997**, *7*, 269−270.

(20) Kong, Q.; Lee, J. H.; Kim, K. H.; Kim, J.; Wulff, M.; Ihee, H.; Koch, M. H. J. Ultrafast X-ray Solution Scattering Reveals Different Reaction Pathways in the Photolysis of Triruthenium Dodecacarbonyl ($Ru_3(CO)_{12}$) after Ultraviolet and Visible Excitation. *J. Am. Chem. Soc.* **2010**, *132*, 2600−2607.

(21) Hunstock, E.; Mealli, C.; Calhorda, M. J.; Reinhold, J. Molecular Structures of $M_2(CO)_9$ and $M_3(CO)_{12}$ (M = Fe, Ru, Os): New Theoretical Insights. *Inorg. Chem.* **1999**, *38*, 5053−5060.

(22) Braga, D.; Grepioni, F.; Tedesco, E.; Calhorda, M. J.; Lopes, P. E. M. Molecular-Structure and Crystal-Structure Generation for $Fe_3(CO)_{12}$. *J. Chem. Soc., Dalton Trans.* **1995**, 3297−3306.

(23) Chakroune, N.; Viau, G.; Ammar, S.; Poul, L.; Veautier, D.; Chehimi, M. M.; Mangeney, C.; Villain, F.; Fiévet, F. Acetate- and Thiol-Capped Monodisperse Ruthenium Nanoparticles: XPS, XAS, and HRTEM Studies. *Langmuir* **2005**, *21*, 6788−6796.